Optimization of Photoresist Plating Mold Fabrication for Metal Mask Patterning

Doreen Hii,[1, a)] Daryosh Vatanparvar,[2] and Andrei M. Shkel[2]
[1)]*Department of Cognitive Sciences, University of California, Irvine, Irvine, CA 92617, United States.*[b)]
[2)]*Mechanical and Aerospace Engineering Department, University of California, Irvine, Irvine, CA 92697, United States.*

(Dated: 23 February 2021)

In this paper, we present results on optimization of PhotoResist (PR) plating molds for patterning of Nickel (Ni) masking layer. The process can be adopted in a number of processes, including Deep Reactive Ion Etching (DRIE) of strongly bonded materials with high chemical resistance, such as Fused Silica (FS), borosilicate glass, and silicon carbide. The desirable plating mold attributes, such as thick PR, controlled dimension, vertical sidewall angle, and low sidewall roughness were optimized by varying exposure dose, exposure contact mode, developer dilution ratio, and PR type. We demonstrated that the PR dimensions decrease proportionally to increase of exposure dose, which relationship was utilized to control fabricated dimensions. To improve the sidewall angle, lowering the exposure dose was shown to reduce sidewall tapering, with further improvements possible by applying the vacuum contact exposure mode. Furthermore, we showed that by using a chemically enhanced PR, such as AZ®12XT, smooth PR sidewalls can be attained. Benefits of optimizing PR features were verified through a FS etch experiment and demonstrated a vertical etch with controlled dimension, smooth sidewall, and reduced faceting.

I. INTRODUCTION

In response to the quest for high performance Micro-Electro-Mechanical (MEM) resonators, research on fused silica (FS) micromachining has gained increasing attention. FS has attractive properties that are essential for realization of high quality factor resonators and operation in harsh environments. Some of the favored properties of FS include high temperature stability to withstand thermal shock, a low thermal expansion coefficient leading to lower thermo-elastic dissipation (TED), and low phonon-phonon mechanical energy dissipation[1–3]. Nonetheless, due to the chemical inertness of FS, patterning into the material poses challenges. Whereas some selected aggressive chemicals such as concentrated hydrofluoric acid (HF) can be used for wet etching of FS material, the imprinted patterns exhibit undesirable undercut profile[1]. In addition, the wet etching process not only suffers from low repeatabiltiy due to its high sensitivity to external variations, such as temperature, concentration, and stirring conditions[4], it also lacks control for etch depth and critical dimensions.

To realize deep anisotropic etching of FS, extensive research has been done using Inductively Coupled Plasma (ICP) to achieve high etch rate, high aspect ratio (ratio of etched depth to width), vertical sidewall, and smooth surface roughness[1,5]. A recent noteworthy result reported $0.57\mu m$/min etch rate, 5:1 aspect ratio etching down to $100\mu m$[6]. Nonetheless, it is an ongoing research to obtain a quality vertical etch profile at high aspect ratio of 10:1 by jointly optimizing over several etch metrics.

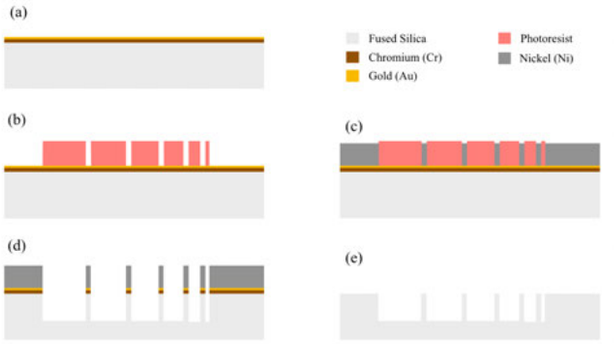

FIG. 1. Process flow for fabrication of FS structures using metal as the etch mask. (a) Deposition of Chromium (Cr) adhesion and Gold (Au) layers for electroplating. (b) Thick PR plating mold patterning. (c) Thick metal mask electroplating to provide adequate protection for the etch process. (d) PR stripping and plasma etching of FS. Defined structure patterns are transferred into the material. (e) Sample after metal removal and substrate cleaning is ready for subsequent processing.

To complement deep FS etching, a highly selective etch mask that can withstand plasma etching is needed. Nickel mask is a popular candidate not only for FS etching, but across etching of strongly bonded material including borosilicate glass[7,8], SiC[9] and Gallium nitride (GaN)[10] because it provides high selectivity to achieve deep etching. A well established procedure for fabrication of high aspect ratio structures is summarized in Fig. 1. A conductive layer is first deposited on FS surface, followed by photolithography (PLG) process that defines patterns of resonator structures. A thick metal layer is electroplated, taking the inverse of the pattern defined by the PR plating mold. After PR is removed, the sample protected by Ni hard mask is etched to transfer the defined pattern into the FS substrate. Subsequent processing, such as

[a)]Electronic mail: doreen.hii@uci.edu
[b)]Work done while affiliated with Mechanical and Aerospace Engineering Department, University of California, Irvine.

metal removal, structure cleaning and releasing is performed to obtain functional resonator structures.

This study focused on optimizing the PR plating mold fabrication, step (b) in Fig. 1. Therefore, this study also relates to plasma etching of other strongly bonded materials besides FS, including borosilicate glass (Pyrex® and Borofloat®) and Silicon Carbide (SiC), where the same process flow, as described in Fig. 1, is also utilized[11–13].

PLG defines patterns to be transferred into the underlying substrate, and the subsequent patterning can only be as good as the defined PR. Therefore, it is important to acquire desired attributes or profiles early in the stage of PLG. For example, to allow for sufficient electroplating of hard mask, the PR plating mold needs to be thick. Ample mask erosion during ICP etching widens etch trenches,[14], or causes faceting[4]. Therefore, it is critical to have a sufficiently thick mask to eliminate consumption of the mask material during the process, which may in turn compromise etch dimensions and profile. Whereas Ni selectivity may be influenced by etch conditions[1], previous studies reported Ni thickness of around $10\mu m$ to be sufficient to provide adequate protection for 10:1 aspect ratio etching down to a depth of $100\mu m$, while balancing for internal stress introduced in thick Ni film[1,15].

The PR dimensions and sidewall angle impact directly the etched profile as it defines the dimension of opening and angle for etching. Fabrication tolerances are tight, especially for MEM resonators, since the natural frequency of the operational mode and the neighboring modes would be affected by uncontrolled etch dimensions, impacting the overall performance of the resonator. As for PR sidewall angle, vertical sidewall can abate etch stop for successful deep $\geq 100\mu m$ high aspect ratio FS etching[15,16].

Defects in mask, such as roughness, would easily transfer to the material in subsequent processing. This plasma-mask interaction has been experimentally verified in previous studies where it was shown that etched sidewalls would follow the same vertical striations as present in the mask[17–19]. Surface defects in resonators, including surface roughness, are known to result in energy dissipation through the surface effects. Surface loss is a major concern in etched FS resonators that affects the total quality factor of a FS resonator and would potentially result in quality factors significantly below the TED limit of the FS material. A smooth PR plating mold is therefore required to minimize etched surface defects by allowing smooth metal mask to be defined.

Fig. 2 illustrates etch defects introduced due to imperfection in PR plating mold, contrasting the results between an ideal case, (1), and four cases with imperfect PR, (2) to (5). In (1), the ideal PR has a good dimensional match, vertical sidewall angle, and smooth surface. The four non-ideal PR cases are: (2) PR with insufficient thickness, (3) PR with uncontrolled dimension, (4) PR with angled sidewall, and (5) PR with rough sidewall surfaces. The definition of a subsequent hard mask takes the inverse of the fabricated PR, perpetuating the imperfections. In (2), thin PR limits the thickness of metal mask, possibly attained since the hard mask thickness cannot exceed that of the PR plating mold. When thin metal mask is unable to provide sufficient protection to sustain the

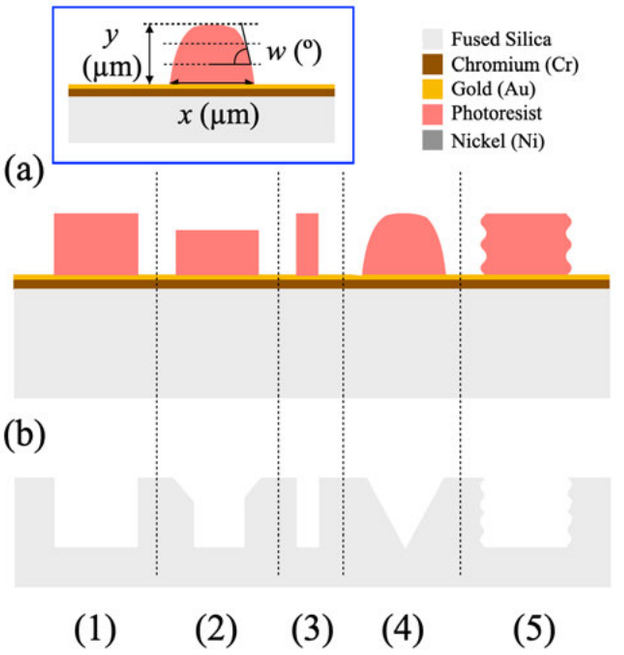

FIG. 2. Summary of etch defects introduced in the etched material due to imperfections in PR plating mold. An ideal PR case, plus four imperfect PR cases, will serve as plating mold for metal mask to be defined, illustrated in (a). Patterned metal mask mirrors the characteristics of its plating mold, propagating imperfections down into the etched materials, shown in (b). Inset: PR evaluation metrics used in this study.

entire etch process, faceting occurs. In (3), mismatched dimension of PR results in mismatched etch opening. Similarly in (4) and (5), tapered PR angle and roughness in PR plating mold is transferred to the metal mask and subsequently into the material, yielding tapered etch and rough etched surface respectively.

We believe in order to fabricate high quality resonators, addressing imperfections in PR plating molds is fundamental. We summarize four desirable PR plating mold attributes imperative for quality etching as follows: (1) thickness: PR thickness should exceed that of target Ni ($10\mu m$); (2) dimensional control: fabricated PR should closely match that of design to minimize fabrication-induced frequency shift of resonators; (3) vertical sidewall angle: promote vertical ion bombardment for anisotropic etching, minimizing faceting; and (4) smooth sidewall: contribute to smoother etched profile, all etch parameters being equal.

However, attributes (1) to (3) are inter-related such that thick PR typically suffers from reduced critical dimension control and tapered sidewall. Since effective exposure dose and develop reaction at the bottom of thick PR is reduced compared to that of the top, this bulk effect demands higher exposure doses and longer developing times[20]. As documented in[21,22], top rounding and non-vertical PR sidewall is common for thick PR, compromising the two attributes that are significant for quality etching.

To exercise control over thick PR fabrication, four sets of

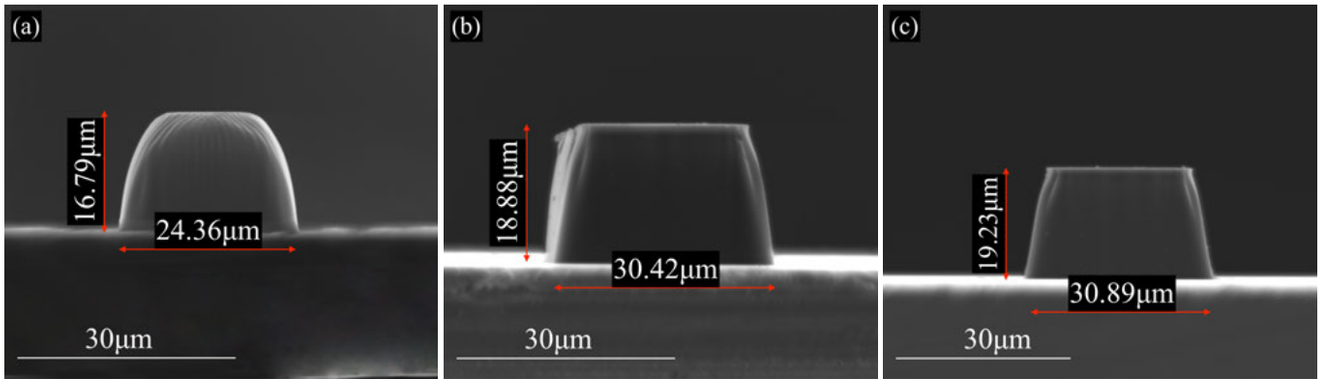

FIG. 3. Cross-section SEM of PR with target dimension of $20\mu m$. Sidewall angle improved as exposure dose decreased. (a) Sidewall angle of 77.15° was obtained when applying an exposure dose of $1600mJ/cm^2$. (b) Sidewall angle improved to 83.12° by reducing the exposure dose to $800mJ/cm^2$. (c) Further reduction in the exposure dose to $400mJ/cm^2$ did not offer additional improvements in sidewall angle as footing was observed.

experiments were conducted manipulating four PLG parameters: exposure dose, exposure contact mode, developer dilution ratio, and PR type. Parameters were specifically tuned to attain attributes in favor of hard mask patterning for deep FS etching. The modulation effect of PLG parameters on the four PR attributes were discussed. Finally, FS etching using hard mask patterned through plating molds with optimized PLG parameters was performed to validate the benefits of optimizing PR on etch profiles.

II. EXPERIMENT

In this study, an optimization of the PR pattern was performed with $15\mu m$ to $18\mu m$ thick extended lines PR on silicon. An outline to the PLG process utilized in this study is as follows: (1) Dehydration bake of wafer in 120°C oven for ≥ 5 minutes for good adhesion of hydrophobic PR to substrate; (2) Priming of wafer surface using adhesion promotor such as hexamethyldisilazane (HMDS); (3) Uniformly dispense thick PR film onto substrate with thickness defined by the spin speed and spin duration; (4) Soft bake in 90 °C oven to solidify PR film with duration dependent on PR thickness; (5) Thorough rehydration of PR film[23] to allow for photochemistry of photoinitiator during exposure; (5) Ultraviolet (UV) exposure of PR to broadband g-, h-, and i-line light source for duration to be optimized using Mask and Bond Aligner (MA6 in our study); (6) Immersion of wafer in developer to remove exposed PR[24].

Fabricated PR patterns were evaluated for sidewall angle, dimension, thickness, and roughness through scanning electron microscope (SEM) cross-sections obtained with FEI Quanta 3D field emission gun (FEG). As illustrated in Fig. 2, w measures PR sidewall angle at the middle section of PR, x measures dimension of PR at the point of contact at substrate surface (bottom of PR), and y measures total thickness of PR. The target PR dimensions were $50\mu m$ width x [10, 20, 30, 50, 100]μm length. Gaps between features were $65\mu m$. Results presented and their effects were verified to hold true for width $500\mu m$ features.

A. Experiment 1: Exposure Dose

Exposure dose was varied (400, 500, 800, 1000, 1200, 1500, and $1600mJ/cm^2$) while applying a soft contact exposure mode. All trials were conducted using positive PR AZ®4620 with developer diluted in water with the ratio of 1:4. Developing times were adjusted accordingly to avoid over-development in the samples located at the center of the wafer, as PR exposed at higher doses are generally easier to develop. Note that for all exposure doses, a complete development of PR was achieved, with the development rate remained consistent at around $0.4\mu m$/min across trials, indicating exposure greater than the minimum dose was applied in all cases[20].

Dimension concordance was assessed by calculating mismatches between target and fabricated PR dimensions ($50\mu m$ x $10\mu m$ and $50\mu m$ x $30\mu m$ features), Δ target (μm) = x - target dimension (x being the dimension of fabricated PR measured at the point of contact of substrate surface, Fig. 2). Fabricated PR dimension decreased linearly in proportion to increase of exposure dose, illustrated in Fig. 4. Sum of Squared Residuals (SSR) of the linear fit ($\Delta\text{target} = -0.005 * \text{Exposure dose} + 4.471$) = 2.87. The equation did not fit the data well at high exposure dose possibly because at excessive exposure dose, bleaching of PR extends into the protected regions, causing rounded top, reducing thickness, and shrinking PR dimension (Fig. 3a). Treating $1600mJ/cm^2$as an outlier, the linear fit $\Delta\text{target} = -0.004 * \text{Exposure dose} + 3.754$ has SSR close to zero, 0.034, indicating a tight fit of the linear model to experimental data.

When evaluated for sidewall angle, a reduced exposure dose was found to improve PR sidewall angle possibly due to a reduced horizontal bleaching in thick PR. When segmenting

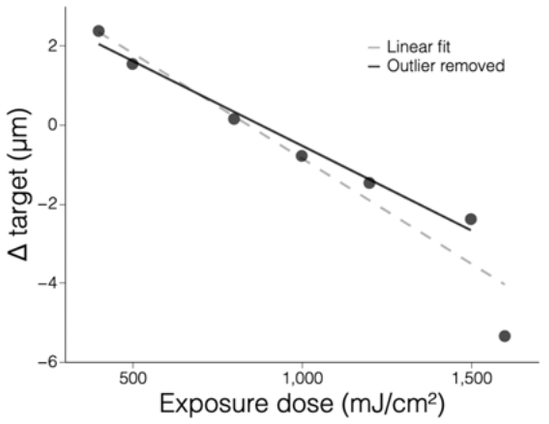

FIG. 4. PR dimension mismatch (Δ target) improved through controlling exposure dose (mJ/cm^2). Fabricated PR dimension decreased linearly in proportion to increase of exposure dose.

PR into three equal sized sections, a minimal change in sidewall angle was found for the bottom-most 1/3 section (consistent to sidewall angle of 83° to 85°), where the exposure wavelength penetrates last; as well as the topmost 1/3 section, where a horizontal bleaching most likely occurred. Reduction in exposure dose improved the middle section of the PR, *w*, Fig. 2. The sidewall angle improved from 77.15° with $1600mJ/cm^2$ to 83.12° with $800mJ/cm^2$. Further reduction to $400mJ/cm^2$, however, did not improve the sidewall profile as footing, widening at the base of PR, occurred. Fig. 3 summarizes the improvement of PR sidewall angle with reducing exposure dose.

B. Experiment 2: Dilution Ratio and Exposure Dose

Two-by-two factorial experiment manipulating exposure dose and developer dilution was performed. Two levels of exposure dose were 1200 and $1500mJ/cm^2$ using soft contact exposure mode; and the two levels of developer dilution were low (1:3 ratio of developer:water) and high (1:4 ratio of developer:water). Each level consisted of five test samples.

PR dimensions (x) were measured and normalized by the target dimension. The resulting Δ targets were analyzed using Bayesian ANOVA[25], with dilution ratio and exposure dose as fixed factors and feature size as a random factor. Analysis provided a strong evidence for exposure dose affecting feature dimensions concordance, $BF_{10} = 7.368$, confirming results from Section II A. Error percentage for Bayesian ANOVA was 0.711%, indicating a good numerical algorithm stability of the analysis. Nonetheless, the optimized exposure dose needs to be coupled with an appropriate developer concentration to preserve intended feature dimensions. A high developer dilution was found to be more suitable. A Bayes factor of $BF_{10} = 128.94$ (error percentage of 1.095%) revealed a decisive evidence of the modulating effect of developer dilution. On average, a dilution ratio of 4 yields PR 1x closer to designed dimension compared to a dilution ratio of 3 regardless of the exposure dose, illustrated in Fig. 5. This is because the decreased dark erosion rate, rate of erosion of unexposed PR, with increasing developer dilution. No interaction was found between the exposure dose and dilution ratio, $BF_{10} = 0.534$. The effects are additive instead of interactive, illustrated in Fig. 5.

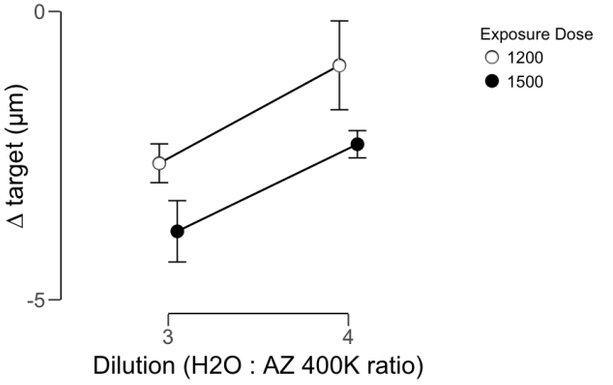

FIG. 5. Main effects of exposure dose and dilution ratio on PR dimension were found. A lower exposure dose increased the fabricated PR dimension to be closer to that of the design; higher developer dilution increased the fabricated PR dimension to be closer to that of design. The two effects are additive: effects are combined when jointly manipulating the two parameters. Error bars indicate 95% credible interval across 5 trials.

When evaluated for PR thickness (y, see Fig. 2), Bayes factor for developer concentration was $BF_{10} = 50.66$, (error percentage of 1.078%), indicating a strong evidence for developer concentration to influence PR thickness. High developer dilution of 1:4 ratio of developer:water provides a better selectivity, with an average thickness of $16.64\mu m$ across 10 trials. On the contrary, the average across 10 trials for low developer dilution of 1:3 ratio of developer:water was $14.97\mu m$, around 10% thinner. Exposure dose was found to have little impact on PR thickness (Bayes factor $BF_{10} = 0.434$, error percentage of 1.595%). Thus, we found an evidence against the interaction between dilution ratio and exposure dose, (Bayes factor $BF_{10} = 0.573$).

Contrary to previous study[22], we did not find evidences for loading effect on sidewall angle during PR development. The sidewall angle remained unchanged for both high and low developer concentrations.

C. Experiment 3: Exposure Contact Mode

In this experiment, the effect of exposure contact mode on PR plating mold profile was studied. Our experiment consisted of two runs of soft and vacuum contact modes, both fabricated using AZ®4620, exposed at the optimal dimension matched and sidewall profile dose of $800mJ/cm^2$ and developed at high developer dilution ratio.

Improvement in sidewall angle was found when the vacuum contact (VA) mode was used instead of soft contact during

the exposure. SEM characterizations indicated a better PR sidewall profile, summarized in Fig. 6. Similarly evaluated at the second 1/3 sidewall section, PR angle improved from 83.12° to 87.82°, when a vacuum contact was applied.

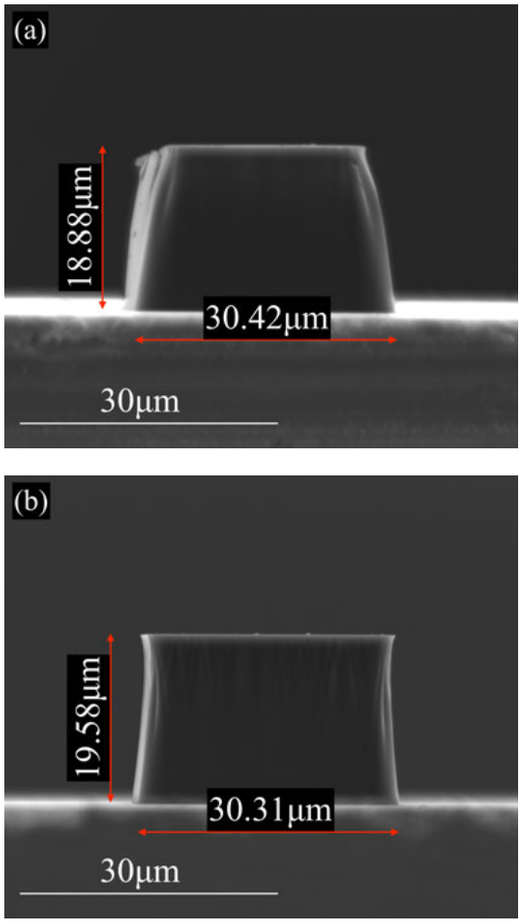

FIG. 6. Cross-section SEM of PR with designed width of 30μm revealing an improved sidewall angle using a vacuum contact exposure mode in (b) as compared to soft contact in (a).

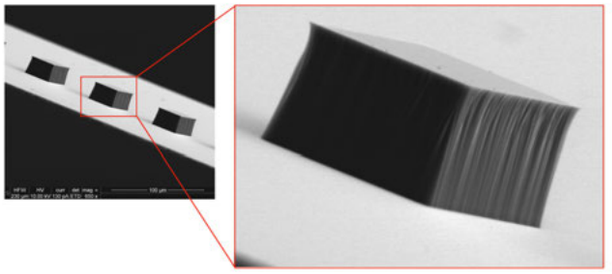

FIG. 7. Cross-section SEM of PR fabricated using AZ®4620 with designed width of 30μm. Note vertical striations along the sidewall.

The vacuum contact provides the finest resolution when compared to other exposure modes of soft, hard and proximity contacts[26]. The vacuum contact differs from other contact modes in that the substrate is located at the closest contact position possible to the mask[27]. The gentle sealing of substrate in the chamber also minimizes trapping of air bubbles between the substrate and mask. In our case, a reduced air gap potentially decreased the diffraction effect of UV light when traveling across different medium, maintaining a vertical bleaching of PR from top to bottom.

D. Experiment 4: Photoresist Type

Two types of positive PRs were compared: AZ®4620 and AZ®12XT. In both cases, PRs were optimized for thickness, best dimension match and vertical sidewall (parameters summarized in Table I).

TABLE I. Summary of PLG parameters utilized to fabricate PR optimized for thickness, dimension match, and sidewall angle for AZ®4620 and AZ®12XT

PLG Parameters	AZ®4620	AZ®12XT
Exposure Dose	$800 mJ/cm^2$	$195 mJ/cm^2$
Exposure Contact	Vacuum contact	Vacuum contact
Developer	1:4 AZ®400T:water	Undiluted AZ®300MIF

SEM characterization was performed to evaluate PR sidewall roughness. In this study, vertical striations were found in all PR features fabricated using AZ®4620. Fig. 7 shows the PR features fabricated using parameters described in Table I. Similar vertical striations were observed in other studies for PR fabricated using AZ®4620: 4.3μm wide x 3.8μm thick PR in[28]; and 20μm x 20μm x 8μm thick PR reported in[29].

One explanation for the PR sidewall roughness is that it might be a texture property of the PR itself and the reaction of PR during the developing step[30,31]. This is a possible explanation since attempts to reduce PR sidewall roughness failed to exert the effect (efforts are summarized below). A smooth PR sidewall fabrication was made possible after we opted a different PR, namely AZ®12XT, shown in Fig. 9.

AZ®12XT is chemically amplified, placing less requirements to initiate photoreaction. Thick AZ®12XT does not need rehydration and can be exposed with only a quarter of the exposure dose needed for AZ®4620. A lower exposure dose also translates into less chance of horizontal bleaching during exposure, resulting in final smooth PR profiles.

Next, we summarize our attempts to obtain smoother sidewall for AZ®4620. Three methods as suggested by previous research were explored, and discussed next.

Since previous studies reported smoother surface after reflow[30,32], hard bake was attempted on the optimized PR with parameters described in Table I. The PR was indeed smoothened after 120°C hard bake for 30 minutes. However, the vertical feature of sidewall was lost due to the introduced rounded profile by the reflow. In addition, the dimension of the bulged PR no longer agreed with the intended design of

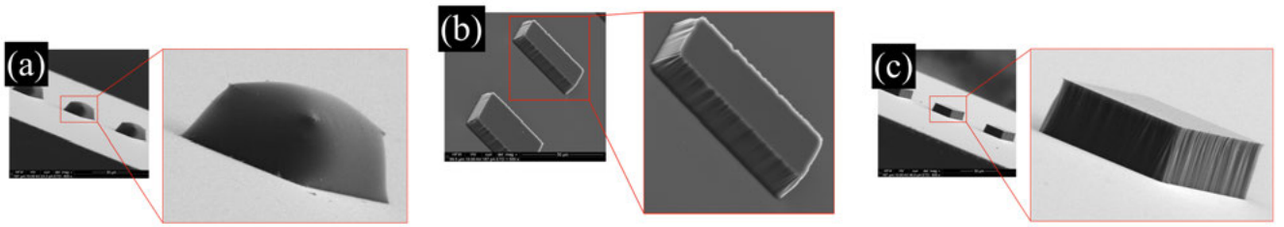

FIG. 8. Efforts investigated to improve PR sidewall roughness. (a) Hard bake smoothed sidewall, but compromised sidewall angle. (b) Minimal sidewall roughness improvement with PEB. (c) Sidewall roughness remained with reduced PR thickness

features (Fig. 8a). In fact, the publication[33] concluded the same noting, that degradation of sidewall angle occurs under the same condition while indeed improvements of sidewall roughness was found. In other words, smooth sidewall with vertical angle after hard bake is impossible, if not hard, to obtain.

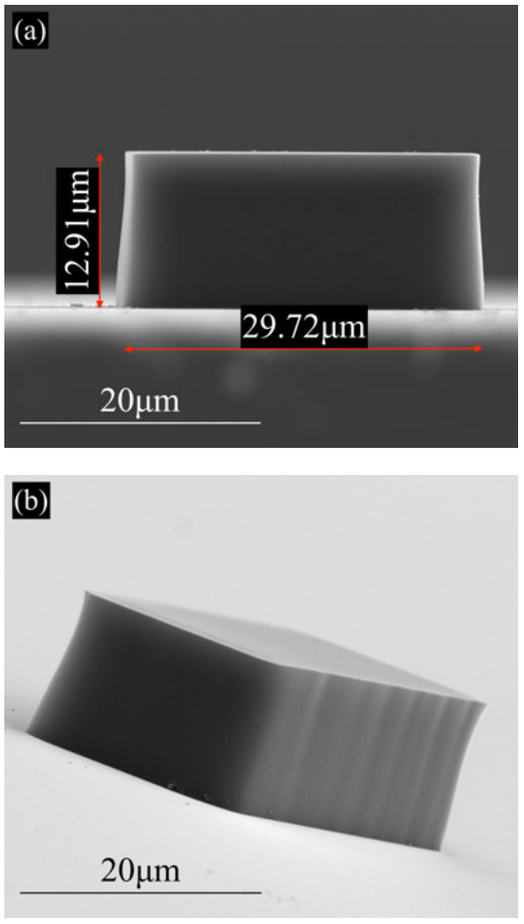

FIG. 9. PR fabricated with AZ®12XT using the optimized recipe in Table I. (a)Fabricated PR with target dimension of 30μm having a sidewall angle of 86.43°. (b) Great reduction in sidewall roughness as compared to PR fabricated using AZ®4620.

We subsequently followed the suggestion in[34], to apply post exposure baking (PEB). Following recommendations in[34], PEB was applied at 65°C for 45s. Nonetheless, vertical striations along PR sidewall were still visible (Fig. 8b). Yet, we explored another approach, proposed in[35], to reduce PR thickness. With lower diffraction effect, a thinner PR was reported to have reduced sidewall roughness. Twelve micrometer (37% thickness reduction) AZ®4620 PR was fabricated with 700mJ/cm^2 vacuum contact exposure and high developer dilution. The sidewall roughness remained even when the PR thickness was reduced (Fig. 8c).

We therefore concluded that hard bake, post exposure bake, or reduction in PR thickness failed to mitigate PR roughness. Future research on the topic might explore other strategies if the objective is to fabricate smooth PR with AZ®4620. In this study, a smooth PR was obtained by using the chemically enhanced AZ®12XT (Fig. 9).

E. Effect of Optimized Nickel Mask on Etching

Following the procedure summarized in Fig. 1, two 500μm thick 4" FS wafers were prepared: (a) Nine micrometer thick Ni was electroplated using optimized vertical smooth AZ®12XT PR plating mold; (b) seven micrometer thick Ni was electroplated using rougher AZ®4620 PR plating mold. Low stress constant current (CC) Ni electroplating was performed at a rate of 0.05μm/min using a current output of 0.1725A and voltage output of 2V. Sulfuric acid based Ni electroplating solution, Ni HT-2 Ready-to-Use (RTU), was maintained at 52 °C ± 1 °C. Wafers were subsequently diced using DISCO DAD3220 Automatic Dicing Saw. Diced samples were cleaned to remove PR and etched at die level using SPTS ICP etcher. The two samples were etched for 240 minutes in the same run using etching parameters summarized in Table II.

Fig. 11 shows etched comparison of features with 30μm x 500μm opening after metal removal. A good dimension match with designed features was obtained. In both cases, the etch openings were close to designed dimensions, with slight widening (within 2μm) as a result of plasma etching. The final etch depth for (a) was 93μm with 88.6° sidewall angle whereas (b) was 89μm with 90° sidewall angle. The

TABLE II. Summary of etch parameters utilized to validate the effect of PR on etch features

Etch Parameters	Values
Antenna Power	1500W
Platen Power	400 W
Platen Temperature	40 °C
C_4F_8 Flow	65 sccm
Ar Flow	75 sccm
O_2 Flow	15 sccm
Chamber Pressure	4 mT

close to vertical sidewall angle indicates that with longer etch time, higher aspect ratio etching can be achieved. Our results also agreed with previous studies[17–19], that roughness in mask is transferred to underlying material during etching. Rough vertical striations were observed for plating mold defined by AZ®4620 and not AZ®12XT.

Typical faceting, as identified by a slanted angle at the top of opening, was found for etch sample (b), where $7\mu m$ thick hard mask was insufficient to sustain the etch process. Whereas faceting was reduced using a thicker Ni mask in (a), it was not fully eliminated. Ni hard mask of $> 9\mu m$ is needed for sufficient protection in future research[4].

F. Limitations

In this study, an array of PR dimensions was explored, including 100, 50, 30, 20, 10, and $5\mu m$. Whereas thickness and roughness were consistent across feature sizes, the magnitude of dimension deviation from design (Δ target) as well as sidewall angle were not consistent. PR thickness relates to uniformity of dispensed PR, whereas roughness may be a property of the PR itself. For feature dimension and sidewall angle, a one-size-fit-all solution might not exist, especially where there are significant variations in feature sizes. The phenomenon was termed process nonlinearity[36], where the research reported a challenge in joint optimization of PR with different feature sizes. Features with dimension $\geq z\mu m$ can be optimized together. Below the threshold, Δ target and sidewall angle deviated enough from the rest, making the simultaneous optimization challenging. The threshold z changes for different PR types and PR thicknesses.

For example, when optimizing for PR using AZ®12XT, the exposure doses of 170, 185, and $195 mJ/cm^2$ were tested. The threshold z for the set of optimization was $5\mu m$ if a tolerance of $\pm 0.5\mu m$ was applied. As illustrated in Fig. 10, features with similar dimensions experienced the effect of a similar magnitude (steepness of slope in the graph) as the exposure dose decreased. Joint optimization (closeness of points in graph) for features $\geq 5\mu m$ was possible, with $\pm 0.3\mu m$ deviation achieved. The dimensional match for $5\mu m$ feature was outside of the tolerance band. The optimal exposure dose for $5\mu m$ is projected to be around $180 mJ/cm^2$.

A change in optimal exposure dose requires the corresponding change in exposure depth of focus to obtain the vertical sidewall angle. The process window, being constrained by both exposure dose and depth of focus, shifts when exposure dose changes[37]. In addition, small features are especially sensitive to this shift[38]. In cases where there is a huge variation in feature sizes across the wafer, the intersection of process windows for large and small features may be tight, making the joint optimization challenging. Therefore, we advise for low variation in feature sizes in resonator designs because the effects of modifying PLG parameters would remain consistent across similar feature sizes.

However, once the optimization has been performed, the results are highly repeatable. For example, four runs of PR using the optimized AZ®12XT recipe on both Si and FS materials had a mean PR dimension of $30.06\mu m$ (SD, $\sigma = 0.244\mu m$), averaged thickness of $13.155\mu m$ (SD, $\sigma = 0.212\ \mu m$), mean sidewall angle of $85.82°$(SD, $\sigma = 0.40°$), and no noticeable variation in roughness.

Note that in Fig. 10, the changes in slope across different exposure dose are more significant for features with target length dimension of $30\mu m$ and $50\mu m$. We believe this is an artifact. Since width of target PR features was fixed at 50m while lengths varied from $5\mu m$ to $100\mu m$, for features with width and length close to $50\mu m$, the slopes encode about two times the effect of exposure dose manipulation.

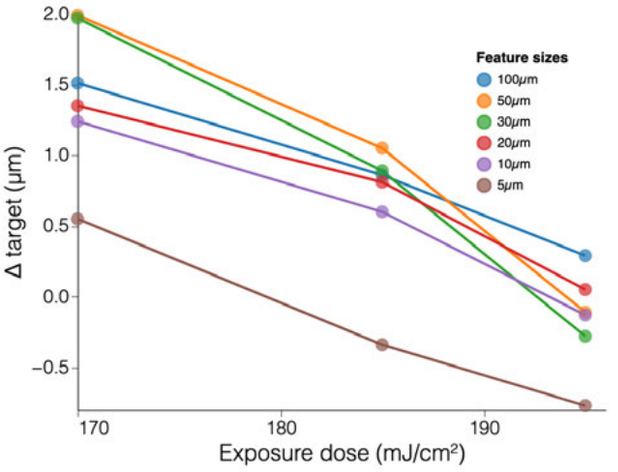

FIG. 10. An example of process nonlinearity when optimizing for $14\mu m$ thick PR using AZ®12XT. Exposure dose of $195 mJ/cm^2$ was optimal for feature sizes $> 5\mu m$, where dimension concordance was $\pm 0.5\mu m$ for all other feature sizes, with $5\mu m$ feature as an outlier.

In this study, the quantitative analysis of Ni profile was not performed, since an extended lines pattern was utilized. Blanket covering of Ni means that cross-section of electroplated Ni cannot be obtained without introducing an external force that would delaminate Ni from the surface. Therefore, it is assumed in the current study that Ni follows the profile defined

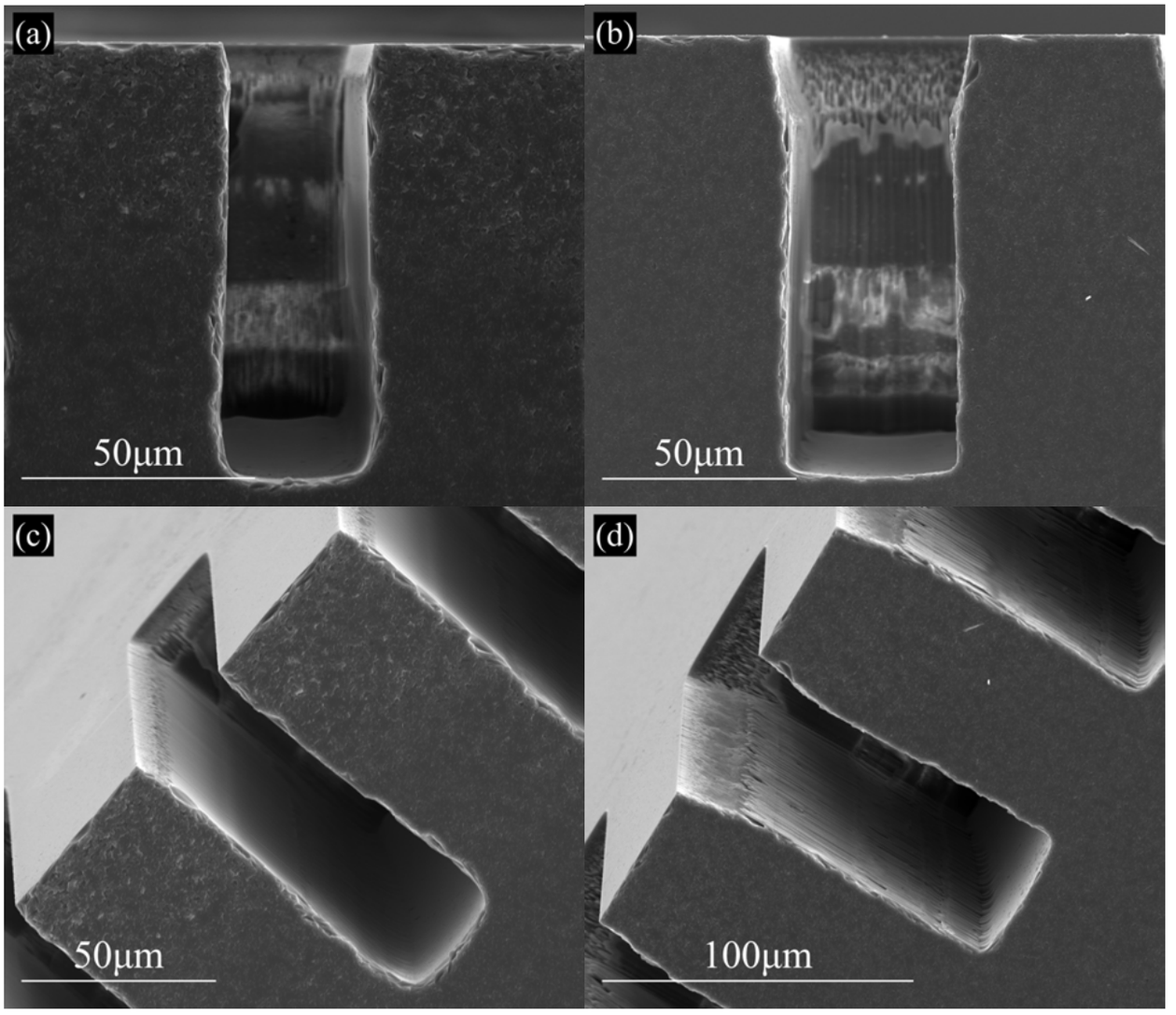

FIG. 11. SEM characterizations of etch features with designed opening of $30\mu m$ x $500\mu m$. (a) and (b) show the cross-section of characterized features; (c) and (d) show sidewalls of the characterized features. (a) Minimal faceting was observed using optimized AZ®12XT lithography parameter. Etch depth was $93\mu m$ with 88.6° sidewall angle. (b) Faceting was observed using optimized AZ®4620 lithography parameter as the thinner mask was not able to sustain the entire etch process. Etch depth was $89\mu m$ with 90° sidewall angle. (c) Smooth etched sidewall obtained from AZ®12XT smooth PR plating mold. (d) Using AZ®4620 PR plating mold, roughness in the form of vertical striations was transferred from mask to the etched material.

by PR.

We also acknowledge that a perfectly vertical and steep PR was not accomplished in this study. Future research may explore the effect of PLG parameter focus of exposure, (as for examples in[22,37,39]).

This study contributes to the realization of high aspect ratio etching to the extend that it minimizes hard mask induced etch defects when all etch parameters are equal. Results of this work should be coupled with optimized etch parameters to enable high aspect ratio etching.

III. CONCLUSION

Four desired attributes for the PR fabricated as plating mold for Ni hard mask platting and subsequently for deep fused silica etching were identified: (1) thick PR, (2) dimension concordance with design, (3) vertical sidewall angle, and (4) smooth sidewall. We concluded that increasing the exposure dose leads to a reduced fabricated dimension in a linear fashion, at the same time improving the sidewall angle moderately. A greater improvement in sidewall angle may be obtained by utilizing the vacuum contact mode during exposure where PR

is exposed at a position closest to the mask. We also concluded that with a better controlled PR thickness, as well as dimension, when a higher selectivity developer dilution ratio of 1:4 (developer:water) is applied, as less removal of unexposed region occurred. Sidewall roughness was mitigated when a different PR, AZ®12XT, was chosen. As suggested in[30,31], PR roughness may be a property of PR itself, and this was our observation as well. The additional efforts such as hard bake, reducing PR thickness, and post-exposure bake fell short to achieve a smooth sidewall roughness.

Additionally, optimizations adopting relationships described in this study were successfully repeated three times on different PRs with varying thickness: $19\mu m$ and $12\mu m$ features using AZ®4620, as well as $14\mu m$ features using AZ®12XT. In all three cases, a good dimension match, verticality of sidewalls and desired thicknesses were achieved for feature sizes above their respective threshold z (all z were ≤ 30 μm). We believe the optimization concepts presented here may be extrapolated, with best results achieved if performing optimization on consistent feature sizes.

FS etching was performed with PR defined using the optimized recipe for AZ®12XT. A good dimension concordance was achieved between designed and etched features, with a slightly larger opening, possibly due to the effect of etching. Thicker PR enabled thicker Ni to be electroplated as the hard mask, reducing the effect of faceting in the final etched sample. A smoother etch profile was also obtained when PR and Ni sidewall were smooth. We conclude that whereas etch parameters play an important role in defining the quality of etched features, the optimal etch condition should be complemented by optimized quality of the PR plating mold. Thick, vertical, and smooth PR plating mold is an indispensable key in achieving high aspect ratio etching of MEM FS resonators with smooth, defect-free etch profiles.

ACKNOWLEDGMENTS

This material is based on work supported by the Defense Advanced Research Projects Agency (DARPA) and U.S. Navy under Contract No. N66001-16-1-4021.

Fabrication was performed at the UC Irvine Integrated Nanosystems Research Facility (INRF).

DATA AVAILABILITY STATEMENT

The data that support the findings of this study are available from the corresponding author upon reasonable request.

[1]Chenchen Zhang and Srinivas Tadigadapa, Sensor. Actuat. A-Phys. **273**, 147 (2018).
[2]Hui Gong, Cheng F. Li, and Zhong Y. Li, in *Laser-Induced Damage in Optical Materials: 1998*, Boulder, CO, United States, 7 April 1999 (SPIE, Bellingham, WA, 1999).
[3]Vladimir Borisovich Braginsky, VP Mitrofanov, and Vladimir Ivanovich Panov, *Systems with small dissipation* (University of Chicago Press, 1985).
[4]M. Huff and M. Pedersen, J. Appl. Phys. **122, no. 2**, 023302 (2017).
[5]Laicun Lin, Xiangmeng Jing, Qidong Wang, Feng Jiang, Liqiang Cao, and Daquan Yu, Microsyst. Technol. **22, no. 1**, 119–127 (2016).
[6]Michael Pedersen and Michael Huff, ECS J. Solid State Sc. **6**, 644–652 (2017).
[7]Xinghua Li, Takashi Abe, Yongxun Liu, and Masayoshi Esashi, J. Microelectromech. S. **11**, 625–630 (2002).
[8]Mohammed J Ahamed, Doruk Senkal, Alexander A Trusov, and Andrei M Shkel, in *2013 IEEE Sensors Conference*, Baltimore, MD, USA, 4-6 November 2013 (IEEE, Piscataway, NJ, 2013).
[9]Karen M Dowling, Ateeq J Suria, Ashwin Shankar, Caitlin A Chapin, and Debbie G Senesky, in *IEEE 28th International Conference on Micro Electro Mechanical Systems (MEMS)*, Estoril, Portugal, 18-22 January, 2015 (IEEE, Piscataway, NJ, 2015).
[10]Liann-Be Chang, Su-Sir Liu, and Ming-Jer Jeng, Jpn. J. Appl. Phys. **40**, 1242 (2001).
[11]Michael Pedersen and Michael Huff, IEEE J. Microelectromech. S. **26, no. 2**, 448–455 (2017).
[12]J.H. Park, N.-E. Lee, Jaechan Lee, J.S. Park, and H.D. Park, Microelectron. Eng. **82, no. 2**, 119–128 (2005).
[13]Karen M. Dowling, Elliot H. Ransom, and Debbie G. Senesky, IEEE J. Microelectromech. S. **26, no. 1**, 135–142 (2017).
[14]Sami Franssila and Lauri Sainiemi, "Reactive ion etching (RIE)," in *Encyclopedia of Microfluidics and Nanofluidics* (Springer New York, 2015) Chap. 1344, pp. 2911–2921.
[15]Christoph Weigel, Eric Markweg, Lutz Müller, Marcel Schulze, Hassan Gargouri, and Martin Hoffmann, Microelectron. Eng. **174**, 40–45 (2017).
[16]Muhammad Jehanzeb Khan, Takashiro Tsukamoto, Muhammad Salman Al Farisi, and Shuji Tanaka, Sensor Actuat. A-Phys. **305**, 111922 (2020).
[17]Y.P. Hsu, S.J. Chang, Y.K. Su, J.K. Sheu, C.H. Kuo, C.S. Chang, and S.C. Shei, Opt. Mater. **27, no. 6**, 1171–1174 (2005).
[18]Zongliang Cao, Brian VanDerElzen, Kevin J Owen, Jialiang Yan, Guohong He, Rebecca L Peterson, Dennis Grimard, and Khalil Najafi, in *IEEE 26th International Conference on Micro Electro Mechanical Systems (MEMS)*, Taipei, Taiwan, 20-24 January 2013 (IEEE, Piscataway, NJ, 2013).
[19]F Ren, SJ Pearton, JR Lothian, CR Abernathy, and WS Hobson, J. Vac. Sci. Technol. B **10, no. 6**, 2407 (1992).
[20]"Basics of microstructuring: Exposure," `https://www.microchemicals.com/technical_information/exposure_photoresist.pdf` (n.d.), accessed: 2020-03-25.
[21]Warren W. Flack, Ha-Ai Nguyen, Jim Buchanan, Elliott S. Capsuto, and Alan Marks, in *Microlithography 2004*, Santa Clara, CA, United States, 14 May 2004, Vol. 5376 (SPIE, SPIE, Bellingham, WA, 2004) p. 1190.
[22]G Flores, W Flack, Elizabeth Tai, and C Mack, in *SPIE's 1995 Symposium on Microlithography*, Santa Clara, CA, United States, 9 June 1995, Vol. 2438 (SPIE, Bellingham, WA, 1993) p. 41.
[23]It has been summarized thoroughly in[40] and[20] that thick PR may fail to develop fully regardless of the amount of exposure dose and development time applied if the PR film is not sufficiently hydrated. Since water is needed to form dissolution promoter in exposed PR, we would like to reiterate the importance of PR rehydration in thick PR fabrication.
[24]Developing time plays critical role in determining the final PR profile. In our experiments, we immersed the PR in developer for 200s, which value was determined after pilot studies. Development time was slowly incremented if features were not fully cleared under microscope inspection.
[25]George EP Box and George C Tiao, *Bayesian inference in statistical analysis*, Vol. 40 (John Wiley & Sons, 2011).
[26]"MA/BA6 high-precision mask and bond aligner," `https://www.suss.com/brochures-datasheets/mask-aligner-ma-ba-6.pdf` (2014), accessed: 2020-03-25.
[27]H. Miyajima and M. Mehregany, IEEE J. Microelectromech. S. **4**, 220–229 (1995).
[28]Surya Cheemalapati, Mikhail Ladanov, John Winskas, and Anna Pyayt, Appl. Optics **53, no. 25**, 5745–5749 (2014).
[29]Cheng-Chung Jaing, Chii-Rong Yang, Chun-Ming Chang, Yung-Hsin Chang, Chao-Te Lee, and Chine-Nan Hsiao, in *Optical Engineering + Applications*, San Diego, CA, United States, 29 August 2008, Vol. 7067 (International Society for Optics and Photonics, SPIE, Bellingham, WA, 2008) p. 70670P.
[30]Gyorgy A. Porkolab, Paveen Apiratikul, Bohan Wang, S. H. Guo, and Christopher J. K. Richardson, Opt. Express **22, no. 7**, 7733 (2014).
[31]Fatima Toor, Deborah L. Sivco, Hao E. Liu, and Claire F. Gmachl, Appl. Phys. Lett. **93, no. 3**, 031104 (2008).

[32]Jhy-Cherng Tsai and Yong-Sung Hsu, IEEE T Magn. **47, no. 3**, 598–601 (2011).
[33]Munirathna Padmanaban, David Rentkiewicz, SangHo Lee, Chisun Hong, Dongkwan Lee, Dalil Rahman, Raj Sakamuri, and Ralph R. Dammel, in *Microlithography 2005*, San Jose, CA, United States, 4 May 2005, Vol. 5753 (SPIE, SPIE, Bellingham, WA, 2005) p. 862.
[34]Qi Chang Li, Guang Long Wang, Jiang Lei Lu, Feng Qi Gao, and Shan Shan Zhang, *Advanced Materials Research*, Adv. Mater. Res.-Switz **538**, 2273 (2012).
[35]T Suligoj, KL Wang, and P Biljanovic, in *IEEE Mediterranean Electrotechnical Conference*, Cairo, Egypt, 7-9 May 2002 (IEEE, Piscataway, NJ, 2002).
[36]Warren W. Flack, Ha-Ai Nguyen, and Elliott S. Capsuto, in *Microlithography 2003*, Santa Clara, CA, United States, 12 June 2003, Vol. 5039 (SPIE, Bellingham, WA, 2003) p. 1257.
[37]Chris A. Mack, "Lithography control and optimization," in *Field Guide to Optical Lithography* (SPIE, 2006) pp. 53–87.
[38]Chris A Mack, in *ISMA '97 International Symposium on Microelectronics and Assembly*, Singapore, 14 August 1997, International Society for Optics and Photonics (SPIE, SPIE, Bellingham, WA, 1997) pp. 14–27.
[39]He Rong Yang, Tang Chun Weng, Wei-Jhe Tzai, Chien-Hao Chen, Chun-Chi Yu, Wei-Yuan Chu, Sungchul Yoo, Chien-Jen Huang, and Chao-Yu Cheng, in *SPIE Advanced Lithography*, San Jose, CA, United States, 19 March 2015, Vol. 9424 (International Society for Optics and Photonics, SPIE, Bellingham, WA, 2015) p. 94242C.
[40]Octavia P. Lehar, Mark A. Spak, Stephen Meyer, Ralph R. Dammel, Colin J. Brodsky, and C. Grant Willson, in *26th Annual International Symposium on Microlithography*, Santa Clara, CA, United States, 24 August 2001 (SPIE, Bellingham, WA, 2001) p. 463.
[41]"Basics of microstructuring: Development," (n.d.), accessed: 2020-25-16.
[42]"Technical datasheet: AZ® 12XT-20PL Series," https://microchemicals.com/micro/tds_az_12xt_photoresist.pdf (2016), accessed: 2020-03-25.